The Journal of Green Energy and Environmental Engineering

Research Paper

Detection of Quinolone Antibiotics by Magnetic Solid-Phase Extraction Coupled with High-Performance Liquid Chromatography Based on Graphene-Conjugated Porous Materials

Gerson Bacher[1], Ricardo Clavijo[1], Navadol Alves[2,*]

[1] Laboratory of Forest Products Chemistry, Helsinki University, P. O .Box 6300, FIN-02015 HUT, Finland.
[2] BOKU-University of Natural Resources and Applied Life Sciences, Vienna, Department of Chemistry, Muthgasse 18, A-1190 Vienna, Austria
*Corresponding author: Alves.n@boku.ac.at

Abstract. An analytical methodology was established for simultaneous determination of four banned quinolone residues through magnetic solid-phase extraction coupled with high-performance liquid chromatographic separation. The extraction sorbent comprised a graphene-derived composite porous architecture (Fe_3O_4@CMP-2). The conjugated microporous polymer precursor (CMP-1) was fabricated via Sonogashira cross-coupling polymerization employing 1,3,5-triethynylbenzene and 4,4'-dibromobiphenyl-2,2'-diamine as comonomers. Subsequently, CMP-2 was prepared by condensing CMP-1 with graphene oxide (GO). The resulting CMP-2 was subjected to systematic structural and morphological characterization. A mixed MSPE adsorbent was prepared via simple physical mixing of CMP-2 and nano-Fe_3O_4 to separate and enrich the four quinolone drugs in food and water samples. Single-factor experiments were conducted to examine the key parameters affecting extraction performance. Under optimized analytical conditions, the developed approach exhibited robust linear response across the 0.050–20.00 μg/L calibration range, with determination coefficients exceeding 0.9961. Method sensitivity, expressed as limits of detection, spanned 0.004–0.022 μg/L. Accuracy assessment via tri-level fortified recovery trials yielded extraction efficiencies between 97% and 118%, with precision characterized by relative standard deviations of 0.02%–2.3%. Compared with similar enrichment methods reported in the literature, this method offers distinct advantages across multiple dimensions: a smaller sample volume, less adsorbent material, short extraction and desorption times, and simpler operation.

Keywords: *Magnetic solid-phase extraction; High-performance liquid chromatography; Quinolone antibiotics; Fe_3O_4; Conjugated microporous polymersn*

Received on 15 Feb 2026, Accepted on 15 April 2026, Published on 02 May 2026

1 Introduction

Extensive therapeutic and prophylactic deployment of antimicrobial agents in livestock production and veterinary practice has precipitated substantial public health apprehensions concerning residual antibiotic contamination in foodstuffs of animal origin and environmental compartments [1, 2]. Among these pharmaceuticals, fluoroquinolone antibiotics (FQs)—such as enrofloxacin (ENR), ofloxacin (OFL), marbofloxacin (MAR), and sarafloxacin (SAR)—are synthetic broad-spectrum antimicrobial agents valued for their efficacy and low cost. Nevertheless, their pervasive utilization has engendered persistent bioaccumulation in meat, ovoproducts, and dairy matrices, presenting severe health hazards to consumers encompassing hypersensitivity responses, antimicrobial resistance propagation, and potential oncogenicity [3, 4]. Accordingly, Chinese National Standard GB 31650-2019 establishes stringent maximum residue thresholds for fluoroquinolones in food commodities (e.g., ≤0.5 μg/kg for enrofloxacin in eggs), mandating the establishment of ultrasensitive and dependable analytical methodologies for contaminant surveillance [3].

Currently, the primary analytical techniques for quantifying FQs in complex matrices include enzyme-linked immunosorbent assay (ELISA), capillary electrophoresis (CE), high-performance liquid chromatography (HPLC),

and liquid chromatography-tandem mass spectrometry (LC-MS/MS) [6–9]. While LC-MS/MS offers superior specificity and sensitivity for multi-residue confirmation, its high instrumentation cost and complex operation limit its routine application in many laboratories. In contrast, HPLC coupled with ultraviolet (UV) or diode-array detection (DAD) provides a more accessible and cost-effective alternative. However, a major bottleneck in the accurate quantification of FQs by HPLC is the complexity of sample matrices—particularly in food samples rich in proteins, lipids, and pigments—which can interfere with chromatographic separation and detection. Therefore, efficient sample preparation techniques that can selectively extract and pre-concentrate trace analytes from complex matrices are essential for improving the sensitivity and reliability of HPLC analysis [10].

Magnetic solid-phase extraction has evolved into a robust sample preparation methodology, integrating the discriminative capacity of conventional solid-phase extraction with the operational convenience of magnetic field-assisted retrieval. By using magnetic nanoparticles (MNPs) as the adsorbent, MSPE eliminates the need for cumbersome centrifugation or filtration steps, significantly reducing processing time and solvent consumption [15]. To achieve high selectivity and adsorption capacity, the surface of MNPs must be functionalized with appropriate coating materials. In recent years, porous organic polymers (POPs), particularly conjugated microporous polymers (CMPs), have attracted considerable attention as adsorbent materials due to their high surface area, permanent porosity, tunable functionality, and excellent physicochemical stability [10–14]. Nevertheless, pristine CMPs often lack the magnetic properties required for facile separation. Although covalent immobilization of CMPs onto magnetic cores is effective, it often involves complex chemical synthesis. A simpler physical mixing strategy to combine the merits of both materials remains desirable.

Graphene oxide is widely recognized for its superior sorptive affinity toward aromatic molecules, mediated primarily through π–π electron donor–acceptor interactions and hydrophobic partitioning. Integrating GO with CMPs can create synergistic adsorption sites that enhance the extraction efficiency of FQs, which themselves possess aromatic quinolone rings [17–19]. Moreover, the introduction of GO may improve the dispersibility of the composite material, facilitating better contact with target analytes in the sample solution.

In this study, we designed and synthesized a novel graphene-conjugated porous material (CMP-2) by covalently linking a GO sheet with a CMP derived from 1,3,5-triethynylbenzene and 4,4′-dibromobiphenyl-2,2′-diamine via Sonogashira coupling. The resulting CMP-2 was physically blended with Fe_3O_4 magnetic nanoparticles to form a magnetic composite adsorbent (Fe_3O_4@CMP-2). The physicochemical properties of the material were characterized in detail. Under optimized magnetic solid-phase extraction parameters, the developed sorbent was deployed for selective retrieval and enrichment of four fluoroquinolone residues (marbofloxacin, ofloxacin, enrofloxacin, sarafloxacin) from milk, egg, and freshwater matrices, with subsequent chromatographic determination via high-performance liquid chromatography-diode array detection. The analytical protocol underwent rigorous validation encompassing linear dynamic range, detection thresholds, repeatability, and trueness, with comparative assessment against previously reported methodologies. This investigation delivers an economically viable, expedient, and ecologically sustainable strategy for ultrasensitive surveillance of fluoroquinolone contamination in foodstuffs and environmental specimens.

2. Experimental Section

2.1 Instruments and Reagents

LC-20AT high-performance liquid chromatograph (Shimadzu Corporation, Japan); EVO-18 scanning electron microscope (SEM, Zeiss, Germany); IR PerkinElmer-65 Fourier transform infrared spectrometer (FTIR, Shandong Oulade Instrument Co., Ltd.); X-ray diffractometer (XRD, Thermo Fisher Scientific, USA); HQT-4 thermal analyzer (TGA, Beijing Hengjiu Experimental Equipment Co., Ltd.); Autosorb IQ fully automatic surface area analyzer (BET, Quantachrome Instruments, USA).

1,3,5-Triethynylbenzene (purity 99%), tetrakis(triphenylphosphine)palladium ($Pd(PPh_3)_4$, purity 98%), copper(I) iodide (CuI, purity 99.5%) (Saen Chemical Technology Co., Ltd.); 4,4'-dibromobiphenyl-2,2'-diamine (purity 99%, Shanghai Haohong Biomedical Technology Co., Ltd.); Marbofloxacin (MAR), Ofloxacin (OFL), Enrofloxacin (ENR), Sarafloxacin hydrochloride (SAR) (analytical grade, Macklin Inc.); Acetonitrile (chromatographic grade, Anergy

Chemical Co.); other reagents were analytical grade (Chengdu Kelong Chemical Co.). Milk and eggs were purchased from local supermarkets; water samples were taken from Jinlong Lake in Chongzuo City.

2.2 Preparation of Conjugated Organic Porous Polymer CMP-2

As shown in Figure 1, intermediate CMP-1 was first prepared, followed by covalent bonding with GO to prepare the graphene-modified composite porous material CMP-2.

Preparation of CMP-1: 1,3,5-Triethynylbenzene (0.40 g, 2.66 mmol), 4,4'-dibromobiphenyl-2,2'-diamine (1.35 g, 3.99 mmol), $Pd(PPh_3)_4$ (0.02 g, 0.017 mmol), and CuI (0.008 g, 0.042 mmol) were dissolved in a solution containing triethylamine (15 mL) and N,N-dimethylformamide (100 mL). The reaction mixture underwent 20 min deaeration prior to thermal polymerization at 95°C under inert nitrogen atmosphere for 48 h. Post-reaction, the system was cooled to ambient temperature and subjected to solid-liquid separation. The isolated solid was sequentially purified via washing with chloroform, deionized water, and acetone. Further purification was achieved through 48 h Soxhlet extraction employing acetone as the eluent. The resultant CMP-1 product was desiccated under vacuum at 60°C for 12 h and retained for subsequent applications.

Synthesis of CMP-2: 0.80 g CMP-1 and 1.50 g graphene oxide were suspended in a binary solvent system comprising 40 mL N,N-dimethylformamide and 40 mL diisopropylamine. The dispersion was heated to 80°C under nitrogen blanket with continuous agitation for 72 h. Following thermal quenching to ambient temperature, the mixture was filtered and the recovered solid exhaustively washed with water, methanol, dichloromethane, and acetone. Purification was completed via 48 h Soxhlet extraction using methanol. The terminal product was vacuum-desiccated at 60°C for 12 h.

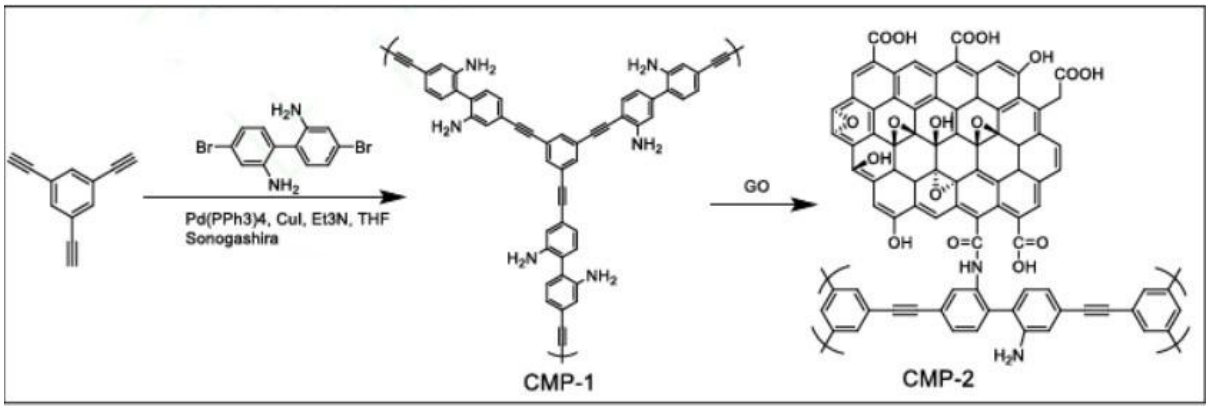

Figure 1 The preparation route of porous polymer CMP-2.

2.3 Chromatographic Conditions

Chromatographic column: Shimadzu C18 column (4.6 mm × 250 mm, 5 μm); Flow rate: 1.0 mL/min; Column temperature: 40°C; Injection volume: 20 μL; Detector wavelength: 280 nm; Mobile phase A: 0.1% formic acid aqueous solution; Mobile phase B: 0.1% formic acid acetonitrile solution. Gradient elution program: 0–6 min, 10%–20% B; 6–25 min, 20%–58% B; 25–30 min, 58%–100% B.

2.4 Standard Curve, Limits of Detection and Quantification

Stock standard solutions at 1.0 mg/mL were prepared and subjected to serial dilution to yield working concentrations of 0.10, 0.50, 1.0, 5.0, 10.0, and 20.0 μg/L. Following membrane filtration (0.22 μm), 20 μL aliquots were chromatographically analyzed to construct calibration functions for each target compound. Method detection limits were established at signal-to-noise ratio of 3, with quantification thresholds defined at S/N = 10.

2.5 Precision

Six replicates of a 10.0 μg/L test solution were prepared and analyzed under the chromatographic conditions described above to calculate the intra-day precision (RSD). For three consecutive days, six replicates of a 10.0 μg/L test solution were prepared daily and analyzed to calculate the inter-day precision (RSD).

2.6 Sample Pretreatment

Milk specimen preparation: 10.0 g milk was transferred to a 50 mL centrifuge vessel and fortified with predetermined fluoroquinolone standard solution. Following equilibration, 10 mL ammonium acetate buffer (10 mmol/L, pH 5.0) was incorporated. The mixture was centrifuged at 5000 r/min for 5 min, the supernatant decanted, and its acidity adjusted to pH 2.0 for subsequent processing.

Egg specimen preparation: Eggs were cracked, shells discarded, and contents homogenized. A 2.0 g aliquot was transferred to a 50 mL centrifuge vessel, fortified with fluoroquinolone standard solution, and combined with 8 mL acidified acetonitrile (1% formic acid). The mixture underwent vortex agitation, 5 min orbital shaking, and centrifugation at 10000 r/min for 5 min. The resulting supernatant was decanted to a fresh 50 mL vessel, with the residual pellet subjected to re-extraction using an additional 8 mL of 1% formic acid-acetonitrile solution. The extracts were combined, blown dry with N_2 at 40°C, reconstituted with 4.0 mL of mobile phase, vortexed, transferred to a 15 mL tube, and centrifuged at 12000 r/min for 5 min. The supernatant was collected, and the pH was adjusted to 2.0.

Water samples: Water samples were filtered through a 0.22 μm membrane to remove suspended particles, spiked with appropriate FQs standards, and the pH was adjusted to 2.0.

2.7 Magnetic Solid-Phase Extraction Procedure

In a 5 mL centrifuge tube, 5.0 mg of CMP-2 and 5.0 mg of magnetic nanoparticles (MNPs) were accurately added, followed by 1.0 mL of methanol. The mixture was vigorously shaken for 1 min to allow full complexation of CMP-2 and MNPs to form magnetic CMPs. An external magnetic field was applied to rapidly adsorb the magnetic CMPs to the tube wall, and the supernatant was discarded to remove uncomplexed small molecule impurities. 2.0 mL ultrapure water was introduced to the vessel and agitated for 1 min to condition the magnetic adsorbent surface (eliminating residual methanol and establishing an aqueous milieu conducive to subsequent analyte retention). Magnetic retrieval was repeated and the aqueous phase discarded to finalize sorbent activation. The sample solution (2.0 mL) containing target fluoroquinolones was then added, with vigorous 5 min shaking to generate a homogeneous dispersion ensuring exhaustive analyte sequestration by the magnetic composite. Post-extraction, the magnetized particles were rapidly isolated via external magnetic field application and the spent supernatant removed. A 3.0 mL ultrapure water rinse was administered with 3 min vigorous agitation to eliminate co-adsorbed matrix constituents, followed by magnetic separation and wash fraction disposal to preclude chromatographic interference during subsequent instrumental analysis. 1.0 mL of 4.0% (V/V) ammoniated methanol solution was added as a desorbent, shaken vigorously with the magnetic CMPs for 1 min to completely desorb the adsorbed FQs into the desorption solution. Following magnetic retrieval, the eluate was collected and concentrated to dryness under gentle nitrogen stream at 35°C. The resulting residue was reconstituted in 100 μL mobile phase with ultrasonic-assisted dissolution. After clarification, 20 μL of the reconstituted extract was subjected to chromatographic separation.

2.8 Molecular Modeling

Fluoroquinolones exhibiting structural homology were selected as molecular probes. Three-dimensional structural data in SDF format were retrieved from the PubChem repository and subsequently converted to PDB coordinates via Open Babel. Energy minimization and geometric optimization of the CMP-2 architecture were executed using Chem3D to generate the receptor conformation. Putative binding cavities between CMP-2 and target antibiotics were identified to define optimal docking search spaces. All molecular docking simulations were conducted employing AutoDock Vina [16] under uniform parameters: 20 binding poses, exhaustiveness of 10, energy window of 4 kcal/mol, with remaining settings at program defaults. Resultant binding geometries and interaction loci between CMP-2 and fluoroquinolone ligands were systematically analyzed.

3. Results and Discussion

3.1 Characterization of Organic Porous Materials

SEM was used to characterize the surface morphology of the two target polymers. As shown in Figure 2a, CMP-1 exhibited a mixed state of bulk solids and small particles with irregular stacking morphology, showing no distinct structural advantages.

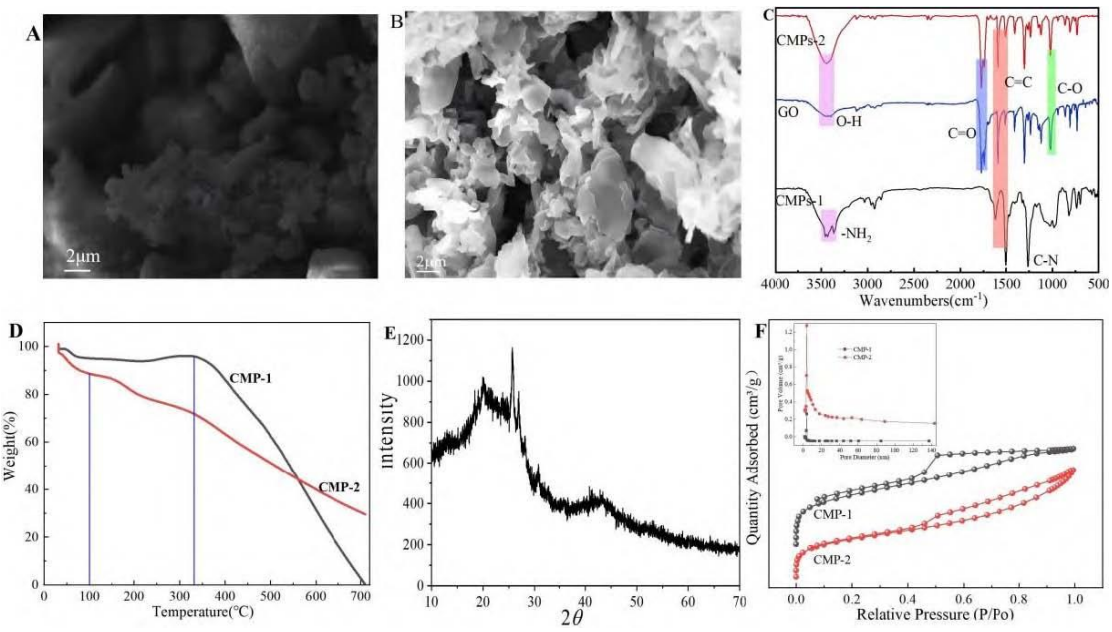

Figure 2 (a) SEM image of organic porous composite CMP-1; (b) SEM image of CMP-2; (c) FT-IR spectrum of CMP-2; (d) TGA of CMP-1 and CMP-2; (e) XRD pattern of CMP-2; (f) Nitrogen adsorption-desorption isotherm of CMP-1 and CMP-2, and pore size distribution plots of CMP-1 (black line) and CMP-2 (red line) (inset).

In contrast, Figure 2b shows significant differences in the micromorphology of the composite material CMP-2, where rich porous structures and flake-like morphologies can be clearly observed. This special morphology offers dual advantages: on one hand, the abundant pore structure provides sufficient adsorption sites and mass transfer channels for adsorption applications, directly enhancing adsorption performance; on the other hand, the flake-like morphology increases the specific surface area, providing stable support for subsequent physical compounding with magnetic Fe_3O_4, ensuring the efficiency of the composite process and the structural stability of the composite product, laying a structural foundation for material function expansion.FT-IR analysis was performed on the polymers, as shown in Figure 2c. For CMP-1, characteristic absorption peaks appearing at 3432 cm^{-1} and 3365 cm^{-1} are attributed to the N-H stretching vibration of amino groups (-NH_2) in its molecular structure. Concurrently, the absorption feature at 1625 cm^{-1} is attributed to N–H in-plane deformation, whereas the band at 1255 cm^{-1} corresponds to C–N stretching within the CMP-1 framework. Upon integration of CMP-1 with graphene oxide yielding CMP-2, both CMP-2 and GO spectra displayed a broadened absorption centered at 3436 cm^{-1}, characteristic of O–H stretching (originating from surface hydroxyl functionalities on GO or atmospheric moisture). Notably, residual amino group signatures from incompletely reacted CMP-1 precursors were absent in the composite spectrum. A prominent carbonyl stretching band emerged at 1742 cm^{-1} in both CMP-2 and GO profiles, unequivocally assigned to C=O vibrations within the GO lattice, confirming successful covalent anchoring of GO to the polymer matrix. Additionally, skeletal C=C stretching modes of aromatic rings appeared at 1593 cm^{-1} and 1500 cm^{-1} across GO, CMP-2, and CMP-1 spectra. The C–O stretching vibration at 1022 cm^{-1}, present in both GO and CMP-2 yet absent in pristine CMP-1, further substantiates GO incorporation into the composite architecture. Comprehensive comparative analysis confirms the successful preparation of polymer CMP-2.

Thermal stability was investigated via thermogravimetric analysis (TGA) (Figure 2d). CMP-1 showed a mass loss of 5% at 320°C, indicating good thermal stability. CMP-2 exhibited an initial weight loss stage below 80°C, primarily due to moisture evaporation. As temperature increased, CMP-2 lost weight rapidly due to the breaking of amide bonds in the GO portion and the decomposition of oxygen-containing functional groups, suggesting that the high-temperature resistance of the amorphous porous polymer connected by amides needs improvement. Since this experiment was conducted at room temperature, this characteristic has little impact. Figure 2e shows the XRD pattern of CMP-2. It can be seen that in the range of $2\theta = 20°–70°$, CMP-2 exhibits only one broad diffraction peak, a characteristic indicating a typical amorphous structure.

To investigate the porous characteristics of the polymers, N_2 adsorption-desorption experiments were conducted at 77.3 K. As shown in Figure 2f, with increasing N_2 pressure, the adsorption amount showed a slow growth trend. Both CMP materials exhibited rapid nitrogen uptake in the low relative pressure domain ($p/p_o < 0.1$). Pore size distribution analysis revealed CMP-1 possessed a characteristic aperture of 3.15 nm, indicative of predominant mesoporosity (Figure 2f inset). Following covalent functionalization with graphene oxide, CMP-2 displayed substantially enlarged pore dimensions of 4.2 nm. BET surface area determination yielded 365.26 m^2/g for CMP-2, representing moderate reduction relative to pristine CMP-1 (463.47 m^2/g), suggesting graphene sheet intercalation partially occluded accessible surface area. However, it is emphasized that CMP-2 still retains a large specific surface area, providing a favorable basis for its application as an adsorbent material in subsequent extraction analysis.

3.2 Optimization of Fe3O4 Nanoparticle Size

To clarify the influence of the magnetic component on the enrichment and separation performance of the composite material, the individual effect of Fe_3O_4 nanoparticles and their compounding mechanism with CMPs were first explored. Results indicated that Fe_3O_4 nanoparticles alone showed no significant enrichment capacity for antibiotics; compounding with CMPs to form magnetic CMP-2 complexes was necessary to acquire both enrichment performance and magnetic separation characteristics. This composite process was achieved by "mixing and oscillating Fe_3O_4 and CMPs in methanol," requiring two key conditions: sufficient Fe_3O_4 dosage to ensure complete separation of all CMP-2 from the matrix solution via magnetic field; and an appropriate Fe_3O_4 particle size to guarantee composite efficiency and separation effectiveness. Based on this, the particle size and dosage of Fe_3O_4 were optimized.

Using "4.0 mg Fe_3O_4 f different sizes (20 nm, 100 nm, 200 nm) + 2.0 mg CMP-2" as the composite system, the mixture was added to a transparent glass vial with methanol. The clarity of the solution and residue at the bottom of the bottle were observed under an external magnetic field to evaluate magnetic separation efficiency. Results showed: Small-sized Fe_3O_4 (20 nm) compounded with CMPs failed to achieve complete separation of CMPs under a magnetic field; a large amount of uncomplexed CMPs remained at the bottom, and the solution appeared significantly turbid. As Fe_3O_4 particle size increased (from 100 nm to 200 nm), the magnetic separation effect of the composite material improved significantly; the solution in the 200 nm Fe_3O_4 group was clear and transparent, with no residue at the bottom. This is because larger Fe_3O_4 particles have a larger physical cross-sectional area, increasing collision probability and physical encapsulation area with CMPs under a magnetic field, allowing rapid capture of CMPs via physical wrapping to achieve efficient separation. This physical composite method avoids complex chemical modification of Fe_3O_4, effectively simplifying the experimental process with both convenience and economy. Considering separation efficiency and operational effectiveness, 200 nm was determined as the optimal particle size for Fe_3O_4 nanoparticles.

Based on the core requirement of "ensuring complete separation of CMPs," the effect of Fe_3O_4 dosage on the formation efficiency of magnetic CMPs was further investigated. By comparing composite and separation efficiencies under different mass ratios (Fe_3O_4:CMPs), it was found that a 1:1 mass ratio not only achieved complete magnetic separation of CMPs but also avoided reagent waste from excess Fe_3O_4 and potential interference in subsequent enrichment processes. In conjunction with the established CMP-2 loading of 5.0 mg, the optimal Fe_3O_4 nanoparticle quantity was ultimately fixed at 5.0 mg.

3.3 Optimization of Extraction Conditions

To systematically optimize antibiotic MSPE conditions for optimal extraction efficiency, sample pH, adsorbent

dosage, extraction time, and desorption conditions (desorbent type, volume, time) were identified as key influencing variables. Single-factor optimization experiments were conducted under a unified condition where the initial antibiotic concentration was fixed at 0.1 μg/L.

Adsorbent dosage directly affects target adsorption capacity and extraction efficiency. Using "5.0 mg Fe_3O_4+ different masses of CMP-2 (1.0, 3.0, 5.0, 7.0, 10.0 mg)" as the composite adsorption system, extraction was performed on 2.0 mL sample solution in a 5.0 mL centrifuge tube, with 1.0 mL of 2.0% (V/V) ammoniated methanol as desorbent. The effect of adsorbent dosage on extraction efficiency was investigated (Figure 3a). It can be seen that when the mass of CMP-2 increased from 1.0 mg to 5.0 mg, the peak areas of the four antibiotics increased significantly, indicating that adsorption sites increased with adsorbent dosage, and extraction efficiency gradually improved. When the mass of CMP-2 further increased to 10.0 mg, peak areas decreased noticeably, presumably because excess adsorbent reduced system dispersibility, hindering effective contact between targets and adsorption sites. Considering method sensitivity and reagent economy, 5.0 mg of CMP-2 was determined as the optimal adsorbent dosage.

Extraction time needs to balance "sufficient target adsorption" and "experimental efficiency." Experiments investigated oscillation time gradients of 3, 5, 7, 10, and 15 min. Figure 3b results show that at an oscillation time of 5 min, the adsorption efficiency of the four antibiotics was highest; prolonging the oscillation time further showed no significant increase in peak area, suggesting that 5 min satisfied the adsorption equilibrium of targets on the adsorbent surface. Based on this, 5 min was selected as the optimal extraction time.

The polarity and acidity of the desorbent directly affect the desorption efficiency of targets from the adsorbent surface. Eight desorbents (1.0%, 2.0%, 3.0% acetic acid methanol; 1.0%, 2.0%, 3.0%, 4.0%, 5.0% ammoniated methanol) were compared. Figure 3c shows that all tested solvents achieved target desorption, but 4.0% ammoniated methanol exhibited the best desorption efficiency, presumably by regulating the interaction between targets and adsorbents (e.g., weakening hydrogen bonding and electrostatic attraction) to promote target desorption. Therefore, 4.0% ammoniated methanol was determined as the optimal desorbent.

After determining the desorbent type, the effect of volume gradients of 1.0, 2.0, 3.0, and 4.0 mL on desorption efficiency was further investigated. Figure 3d results indicate that at a desorbent volume of 1.0 mL, the desorption efficiency for the four antibiotics was highest; exceeding 1 mL caused a decline in desorption efficiency, possibly due to excessive desorbent diluting target concentration and reducing response. Accordingly, 1 mL was selected as the optimal desorbent volume.

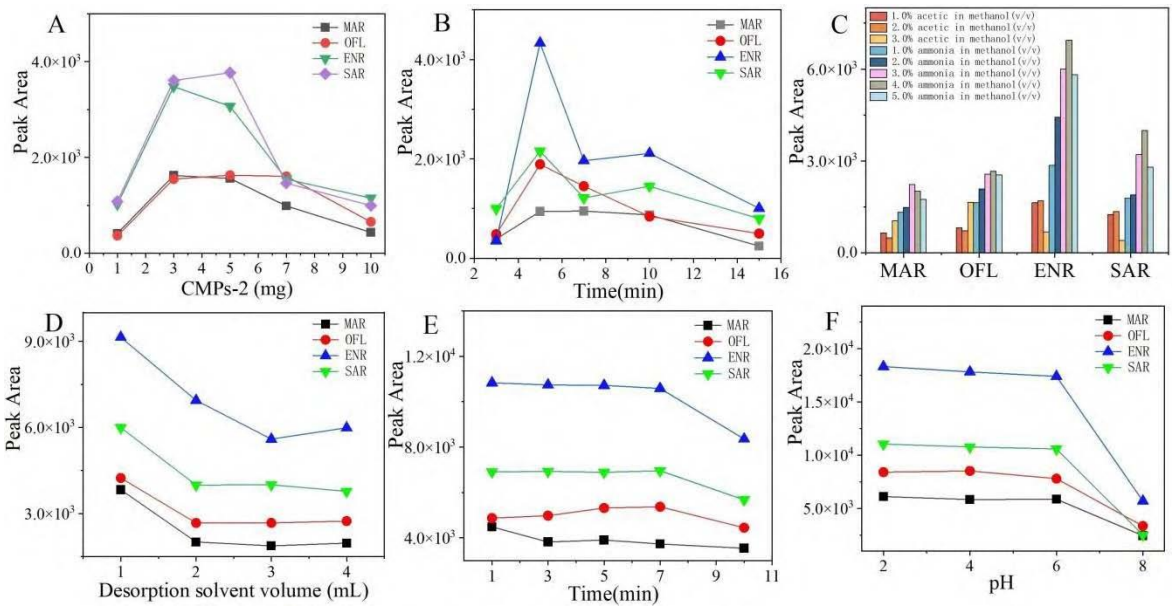

Figure 3 Optimization of operating conditions for MSPE (A) Adsorbent dosage CMP-2; (B) Extraction

time; (C) Type of desorb agent; (D) Dosage of desorb agent; (E) Desorption time; (F) pH of extraction solution. MAR: Marbofloxacin; OFL: Ofloxacin; ENR: Enrofloxacin; SAR: Sarafloxacin hydrochloride.

Experiments set desorption time gradients of 1–10 min to explore the time balance for target desorption (Figure 3e). Results showed no significant difference in desorption efficiency within 1–7 min, indicating that 1 min was sufficient for complete target desorption. To balance experimental speed and desorption effect, 1 min was determined as the optimal desorption time.

Sample pH alters the existing form of targets (e.g., protonation/deprotonation) and adsorbent surface charge via the Henderson-Hasselbalch principle, changing extraction efficiency. HCl and NaOH were used to adjust sample pH from 2.0 to 8.0. Extraction was performed in a "5.0 mg Fe_3O_4(200 nm) + 5.0 mg CMP-2" system with 2.0 mL milk sample, using 1.0 mL of 4.0% (V/V) ammoniated methanol as desorbent. Figure 3f results show that as pH increased from 2.0 to 8.0, the extraction efficiency of the adsorbent for the four antibiotics gradually decreased; at pH 2.0, extraction efficiency was highest. It is speculated that under this condition, targets exist in a protonated form, forming stronger electrostatic attraction with negative charge sites on the adsorbent surface, promoting adsorption. Therefore, pH 2.0 was determined as the optimal sample pH.

3.4 Reusability of the Material

The reuse performance of magnetic CMPs was investigated. After completing one full MSPE cycle under optimized conditions, 3.0 mL of ultrapure water was added, shaken vigorously for 3 min to clean the material, the supernatant discarded, and the material reactivated with methanol and secondary water for the second extraction cycle. This was repeated 6 times to investigate material reusability. As shown in Figure 4, after 6 extraction cycles, recovery rates showed no significant change, indicating good stability of the material during sample processing; reuse was achievable simply through straightforward treatment.

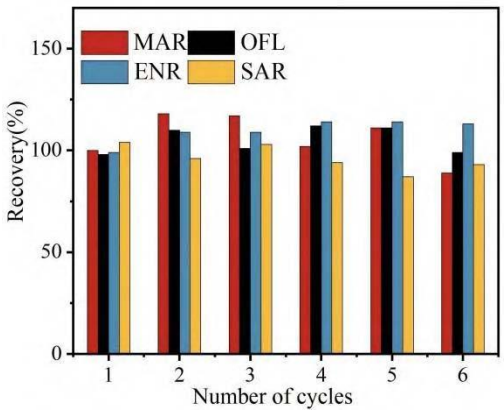

Figure 4 Reusability of magnetic CMP-2. MAR: Marbofloxacin; OFL: Ofloxacin; ENR: Enrofloxacin; SAR: Sarafloxacin hydrochloride.

3.5 Inference of Adsorption Mechanism

The core driving force of the adsorption process is closely related to the environmental system, while pH and solvent composition are key factors affecting adsorbent surface charge, analyte speciation, and their interactions [17]. Therefore, the effects of pH changes in pure aqueous solutions and different methanol content solvent systems on the adsorption of quinolone antibiotics by magnetic CMP-2 were investigated to reveal the adsorption mechanism.

The influence of solution acidity on fluoroquinolone retention efficiency was systematically evaluated by modulating the pH of aqueous media (Figure 5a). Results show that pH significantly regulates the adsorption effect. In acidic environments (pH < 6.0), FQs mainly exist as cationic species [17], experiencing strong electrostatic attraction with carboxyl groups (-COOH) on the GO surface within magnetic CMP-2, hence the material exhibits high adsorption capacity. As pH increases, FQs gradually transform into anionic species, not only weakening electrostatic attraction with carboxyl groups but potentially causing electrostatic repulsion;

simultaneously, incompletely reacted amino groups (-NH_2) undergo protonation (-NH^{3+}), which could form weak electrostatic attraction with antibiotic anions, but this interaction is extremely weak due to the extensive coverage of amino groups by GO, ultimately leading to a significant decline in adsorption capacity as pH increases.

Notably, under acidic conditions, high adsorption efficiency cannot be fully explained by electrostatic attraction alone; other synergistic interactions are presumed. Therefore, the influence of solvent composition was further investigated. By changing the volume fraction of methanol in the adsorption solvent, its effect on adsorption efficiency was analyzed (Figure 5b). Results indicate that as methanol volume fraction increased, the adsorption rate of antibiotics by magnetic CMP-2 gradually decreased. This phenomenon directly confirms the existence of hydrophobic interactions between the material and FQs—methanol, as a polar solvent, weakens hydrophobic interactions, leading to reduced adsorption capacity; even in pure methanol solvent, the material retained some adsorption capacity.

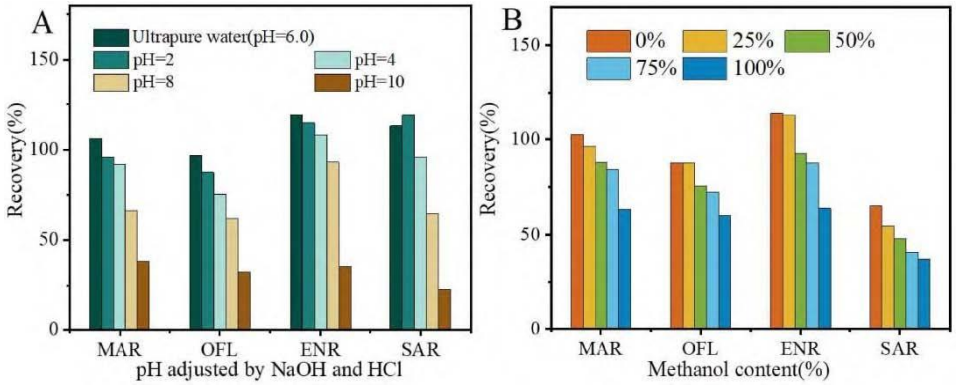

Figure 5 (a) Recovery of four quinolone antibiotics in solutions with different pH; (b) Recovery of four quinolone antibiotics in solvents with different methanol contents.

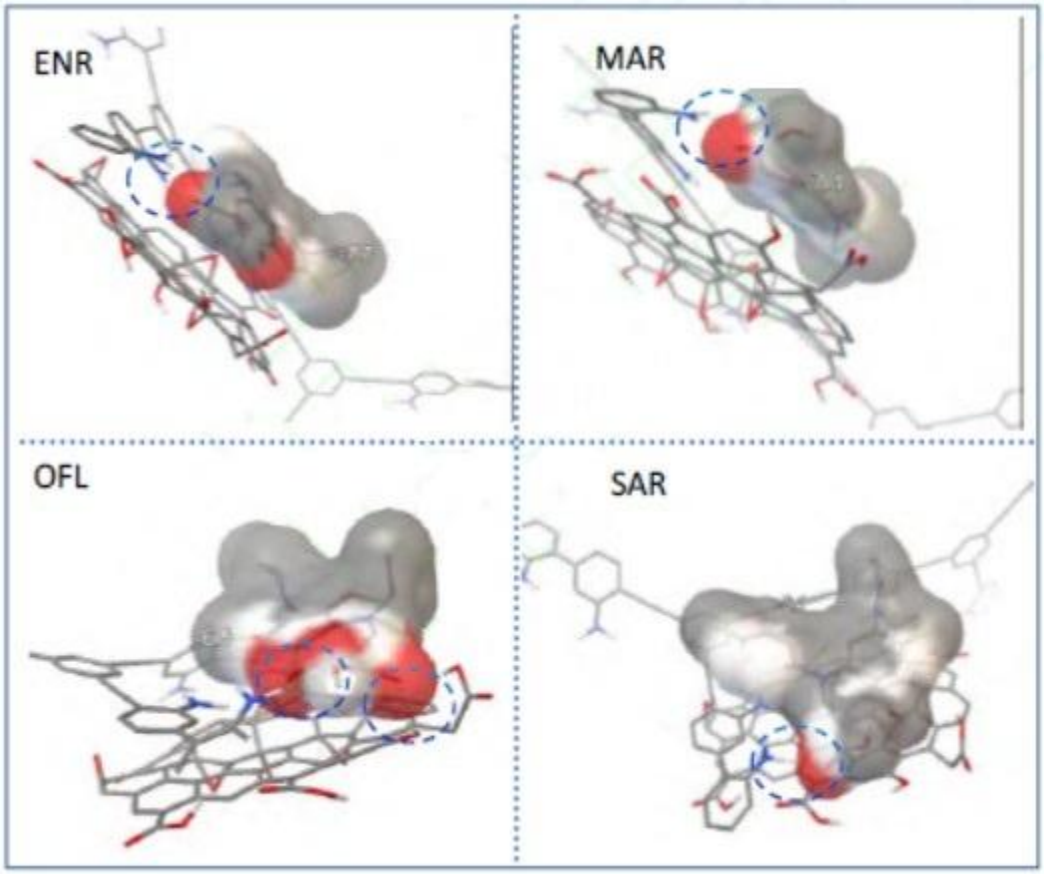

Figure 6 FQs binding modes with CMP-2 (Green dotted line represents hydrogen bonding interaction between CMP-2 and FQs, and the figure number represents binding energy, kcal/mol).

Combined with literature [18–19], the dissociation degree of ionic compounds in organic solvents is extremely low, and electrostatic interactions are negligible; FQs molecules contain quinoline ring structures with strong hydrophobicity. Furthermore, AutoDock Vina was used to analyze the theoretical binding modes of CMP-2 and FQs (Figure 6). All FQs showed good binding modes with CMP-2. FQs molecules interact with CMP-2 in a "parallel" manner similar to GO, with main interaction sites forming strong hydrogen bonds between the carbonyl O of FQs and the N-H of CMP-2 and O-H of GO, with binding energies ranging from -6.9 to -8.1 kcal/mol. This indicates not only π-π hydrophobic interactions between FQs and CMP-2 but also hydrogen bonding during the extraction process. Meanwhile, considering that CMP-2 itself is a porous polymer with a specific surface area of 365.26 m^2/g, its pore size also reflects the auxiliary adsorption effect of the material on FQs molecules. According to Figure 2f, the pore size distribution of CMP-2 is mainly at 4.2 nm. Gaussian09 was used to optimize FQs molecules (PBEPBE method, def2-TZVP basis set), and Multiwfn [20] was used to calculate the volume of FQs molecules. The length of the four FQs is 1.2–1.8 nm, width 0.8–1.3 nm, height 0.4–0.7 nm, indicating that target substances can enter the material interior smoothly.

In summary, the adsorption process of FQs by magnetic CMP-2 is not driven by a single interaction but a combination of electrostatic attraction, hydrogen bonding, hydrophobic interaction, and size-matching effects. Specifically, FQs in solution are adsorbed onto the CMP-2 surface via hydrogen bonding, strong hydrophobicity, and π-π interactions. Simultaneously, the micro/mesoporous structure of CMP-2 provides a high specific surface area, offering abundant sites for FQs adsorption. After FQs fully occupy the outer surface adsorption sites of CMP-2, remaining FQs are transported to the mesoporous region and achieve adsorption via mesopore filling effects.

3.6 Method Performance Evaluation

To systematically verify the analytical performance of the established MSPE-HPLC-DAD method, a series of gradient concentration FQs standard solutions (0.05, 0.10, 0.50, 1.0, 5.0, 10.0, 20.0 μg/L) were analyzed by HPLC under optimized extraction conditions to investigate the linear range, limits of detection (LOD), limits of quantification (LOQ), and reproducibility.

Standard curves were plotted with the concentration of the four target antibiotics as the abscissa and the corresponding HPLC peak area as the ordinate for linear regression analysis; LODs and LOQs were calculated based on signal-to-noise ratios (S/N) of 3 and 10, respectively; intra-day (same batch, n=6) and inter-day (different batches, n=6) parallel determinations over three consecutive days were performed to calculate relative standard deviations (RSD) to evaluate method reproducibility and stability.

Results are shown in Table 1. The four target analytes demonstrated robust linearity across the 0.05–20.0 μg/L calibration range, with determination coefficients spanning 0.9961–0.9991, attesting to consistent proportional response. Method detection and quantification thresholds were 0.004–0.022 μg/L and 0.007–0.075 μg/L, respectively. Intra-assay and inter-assay precision, expressed as relative standard deviations, ranged from 1.6% to 4.6%, confirming exceptional reproducibility and analytical stability. The achieved detection limits substantially surpass the sensitivity requirements of national standard GB 31650-2019 (5–100 μg/kg), demonstrating superior trace-level detection capability adequate for stringent low-concentration antibiotic residue quantification.

Table 1. Performance of MSPE-HPLC-DAD methods for analyzing 4 antibiotics.

Analyte	Linear range/(μg/L)	Linear equation	R2	LOD/(μg/L)	LOQ/(μg/L)	RSD/% Intra-day (n=6)	Inter-day (n=6)
MAR	0.05-20.0	y=30463.963x−5509.32	0.9991	0.022	0.075	1.6	3.5

OFL	0.05-20.0	y=43055.373x−4001.49	0.9988	0.004	0.046	2.1	4.3
ENR	0.05-20.0	y=58100.451x+12906.49	0.9961	0.014	0.049	2.3	4.5
SAR	0.05-20.0	y=50079.731x+16173.26	0.9974	0.005	0.007	2.2	4.6

A comprehensive performance benchmarking of the developed MSPE-HPLC-DAD methodology against previously published approaches for fluoroquinolone residue determination in food matrices was conducted, with comparative metrics summarized in Table 2. As shown in Table 2, the core detection indicators of this method meet or exceed most reported methods: Firstly, the method recovery rate is 97.3%–118.7%, RSD ≤ 5%, both key indicators satisfying the technical requirements for quantitative analysis of FQs residues in food and complying with GB 31650-2019 and related testing standards; Secondly, the method detection limit is as low as 0.004 μg/L, meeting the detection requirements for trace FQs residues with broader applicability.

As shown in Table 3, the operational efficiency of this method is further highlighted: (1) The enrichment requires only 5.0 mg of extraction material, reducing the amount by 75%–90% compared to some reported methods (20–50 mg), greatly reducing costs; (2) The sample volume required for enrichment is ≤20 mL, reducing by 40%–60% compared to some reported methods (35–50 mL), not only lowering the risk of matrix interference during sample pretreatment but also reducing the demand for test samples; (3) High analysis efficiency, with single sample extraction, analysis, and resolution taking ≤1 min, extraction equilibrium time ≤5 min. Combined with the rapidity of the MSPE process (total pretreatment time ≤30 min, no large amounts of organic reagents), the overall analysis cycle is shortened by about 80% compared to traditional methods, truly realizing "fast + efficient" detection of FQs residues. Therefore, the MSPE-HPLC-DAD method established in this study has significant application advantages and practical significance in the field of FQs residue detection in food, providing a new technical choice for food quality and safety control.

Table 2. Comparison of this method with those reported in the literature for determining quinolone antibiotics.

Matrix	Adsorbent	Method	LOD/(μg/L)	Linear range/(μg/L)	Reference
Egg	Fe3O4-MoS2	MSPE-HPLC-UV	0.2-5.0	2.5-300	[21]
Egg	MIP-VTTS-MGO@SiO2	MSPE-DLLME-HPLC-UV	0.011-0.015	0.05-10	[27]
Milk, river water	RAM-MIPs-NH2-MIL-125(Ti)	RAM-MIPs-DSPE-HPLC-UV	0.93-3.15	5.0-200	[22]
Water	SiO2/MnFe2O4	MSPE-HPLC-UV	12-23	4.0-1000	[23]
Milk	CF-Fe3O4-MnO2	DSPE-HPLC-UV	2.3-6.4	5.0-10000	[24]
Water	MDNs	MSPE-HPLC-UV	≤0.06	0.25-500	[25]
Surface water	BA-PVD	MSPE-HPLC-UV	0.05-0.12	0.25-200	[26]
Milk, Egg, Lake water	Fe3O4-CMP	MSPE-HPLC-DAD	0.004-0.022	0.05-20	This work

RAM: Restricted access media; CF: carbon fiber; MDNs: maltodextrin nanosponges; BA-PVD: Boronic acid functionalized magnetic nanoparticles modified with poly(4-vinylphenylboronic acid-divinylbenzene); COF: covalent organic framework; MIP: molecularly imprinted polymer; DLLME: dispersive liquid-liquid microextraction; MIP-VTTS-MGO@SiO_2: MIP based on magnetic graphene oxide embellished with mesoporous silica modified with vinyl groups.

Table 3. Comparison of the performance of the adsorption material in this paper with those reported in the literature for MSPE.

Extraction technique	Adsorbent/amount	Desorption volume/mL	Reuse/times	Desorption time/min	Extraction time/min	Reference

MSPE	Fe3O4@SiO2@P(VI-co-DB)/50 mg	0.5	/	30	30	[29]
MSPE	BA-PVD/30 mg	0.5	30	5	12	[26]
MSPE	MDNs-Fe3O4/5 mg	0.3	7	10	25	[25]
MSPE	MIP-VTTS-MGO@mSiO2 /20 mg	0.05	5	6	12	[27]
MSPE	CMP-2/5 mg	1	6	1	5	This work

3.7 Actual Sample Analysis

Using milk, eggs, and lake water as actual samples, the feasibility of this method was evaluated in combination with HPLC analysis. HPLC chromatograms of actual sample solutions and actual sample solutions spiked with 4 antibiotics (standard addition method) are shown in Figure 7. Eggs contained a small amount of antibiotics, with the content of ofloxacin, enrofloxacin, and marbofloxacin all close to 0.1 μg/L, indicating food safety issues deserve attention. Lake water samples all detected the target substances with high content, especially MAR reaching 0.24 μg/L, indicating slight pollution of surface water. At the same time, the reliability of the method was verified through spike recovery experiments. Results in Table 4 indicate satisfactory spike recoveries (97%–118%).

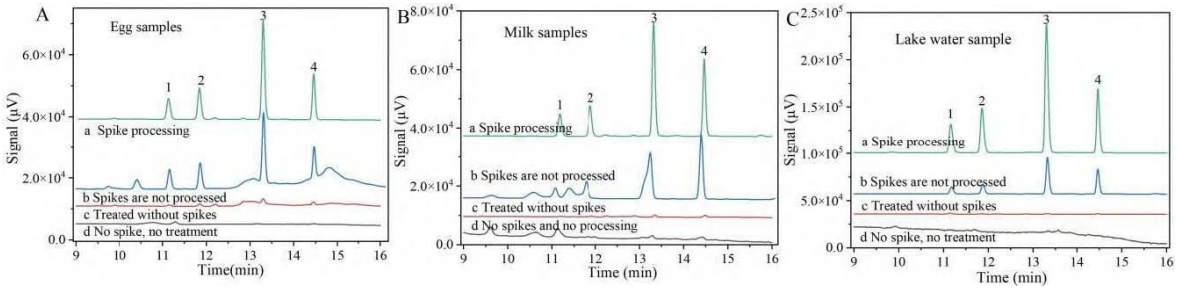

(a: spiked processing; b: spiked 5.0 μg/L unprocessed; c: unspiked; d: unspiked and unprocessed)Chromatographic peaks: 1: Marbofloxacin; 2: Ofloxacin; 3: Enrofloxacin; 4: Sarafloxacin hydrochloride.

Figure 7 Chromatograms of actual samples of (A) egg, (B) pure milk, and (C) lake water after different treatments.

Table 4. Test results of four antibiotics in actual milk, egg, and lake water samples (n=6).

Samples		MAR	OFL	ENR	SAR
Milk	Found	NDd	NDd	NDd	NDd
	Mean recoverya±RSD/%	112.3±0.59	111.2±1.34	115.1±0.21	103.7±1.19
	Mean recoveryb±RSD/%	112.6±0.73	109.3±0.24	111.8±0.16	106.6±1.21
	Mean recoveryc±RSD/%	109.0±0.22	108.8±0.1	107.6±0.13	107±0.48
Egg	Found	0.104±0.02	0.107±0.03	0.098±0.02	0.026±0.02
	Mean recoverya±RSD/%	117.8±2.32	97.3±1.58	102.8±0.82	105.5±0.84
	Mean recoveryb±RSD/%	106.4±0.41	105.3±0.67	107.0±0.14	107.9±1.47
	Mean recoveryc±RSD/%	118.1±0.34	117.0±0.44	116.4±0.24	117.4±0.55
Lake water	Found	0.244±0.01	0.089±0.04	0.084±0.02	0.008±0.01
	Mean recoverya±RSD/%	111.2±1.3	115.2±1.7	118.7±0.72	107.5±0.2
	Mean recoveryb±RSD/%	118.7±1.72	106.9±0.86	105.4±0.17	108.6±0.9
	Mean recoveryc±RSD/%	101.3±0.06	101.7±0.12	101.1±0.14	102.4±0.49

a: Recovery of spiked 0.8 μg/L; b: Recovery of spiked 1.5 μg/L; c: Recovery of spiked 5 μg/L; d: Not detected.

4. Conclusion

In this paper, a GO-modified conjugated microporous polymer material CMP-2 was designed and prepared, and its structure and microporous characteristics were characterized. Furthermore, magnetic organic porous composite adsorbent materials were prepared by physically blending nano-Fe_3O_4 with it, serving as magnetic solid-phase extraction adsorbents. Investigations concerning the preconcentration, isolation, and determination of quinolone antimicrobials in freshwater, dairy, and ovoproduct matrices were undertaken, culminating in establishment of an integrated magnetic solid-phase extraction-high-performance liquid chromatography-diode array detection protocol for fluoroquinolone surveillance across these three sample types. MSPE conditions were optimized and compared with literature methods. This method possesses advantages such as low sample volume requirement, low material dosage (5.0 mg), short extraction time (5 min), short desorption time (1 min), and simple operation, making it suitable for the separation and detection of antibiotics in milk, egg, and lake water samples.

References

[1] Yang C, Wu T. A comprehensive review on quinolone contamination in environments: current research progress[J]. Environmental Science and Pollution Research, 2023, 30: 48778.

[2] Pranjit B, Saptarshi R, Ahmaruzzaman M. Environmental fate of complex antibiotics in aquatic systems and its degradation by electrochemical advanced oxidation process: a holistic review of process variables, mechanistic insights, and implications[J]. Journal of Environmental Chemical Engineering, 2025, 13(6): 120267.

[3] Chen L, Meng X Y, Zhou X H, Wang J Y, Fu Y J, Wang S, Ma Y K, Shen Z Y. New insights into the distribution and risk of antibiotics: From point to non-point source in a rapidly urbanizing watershed—a case study of the Wenyu river, Beijing[J]. Journal of Cleaner Production, 2025, 534: 147085.

[4] Chen X Q, Cai D X, Shen X W, Liao Y N, Ren D X, Ding T. Exploring the changes in chicken manure bacterial community structure and function after antibiotic and composting: Implications for food safety[J]. Food and Humanity, 2025, 4: 100571.

[5] Wu Q, Shabbir M, Peng D, Yuan Z, Wang Y. Microbiological inhibition-based method for screening and identifying of antibiotic residues in milk, chicken egg and honey[J]. Food Chemistry, 2021, 363: 130074.

[6] Zhang B, Lang Y, Guo B, Cao Z, Cheng J, Cai D, Shentu X, Yu X. Indirect competitive enzyme-linked immunosorbent assay based on broad-spectrum antibody for simultaneous determination of thirteen fluoroquinolone antibiotics in Rana catesbeianus[J]. Foods, 2023, 12: 2530.

[7] Hancu G, Papp L A, Szekely-Szentmiklosi B, Kelemen H. The use of antibiotics as chiral selectors in capillary electrophoresis: a review[J]. Molecules, 2022, 27(11): 3601.

[8] Zhu Y G, He P F, Hu H M, Qi M Y, Li T G, Zhang X N, Guo Y M, Wu W Y, Lan Q P, Yang C C, Jin H B. Determination of quinolone antibiotics in environmental water using automatic solid-phase extraction and isotope dilution ultra-performance liquid chromatography tandem mass spectrometry[J]. Journal of Chromatography B, 2022, 1208: 123390.

[9] Mejias C, Santos J L, Martin J, Aparicio I, Alonso E. Automatised on-line SPE-chiral LC-MS/MS method for the enantiomeric determination of main fluoroquinolones and their metabolites in environmental water samples[J]. Microchemical Journal, 2023, 185: 108217.

[10] Wu W P, Li X W, Wei G, Sui L, Xu H, Song Z H. Application of functional materials in separation and analysis of antibiotics[J]. Chinese Journal of Analysis Laboratory, 2025, 44(4): 609.

[11] Ma X Y, Gao Y, Yuan R R. Recent advances in porous organic polymers for electrocatalysis[J]. Technology & Development of Chemical Industry, 2025, 54(10): 54.

[12] Zhang Z, Lu J R. Research progress of photocatalytic reduction of CO_2 by triazine based porous organic polymers[J]. New Chemical Materials, 2025, 53(4): 33.

[13] Li Y, Sun Z J, Hu X, Ren G J, Sun L, Chu S S, Sun L J, Gong W T. Synthesis of novel fluorescent organic porous polymers and sensing of paraquat aqueous solution[J]. Spectroscopy and Spectral Analysis, 2025, 45(10): 2767–2773.

[14] Fu R J, Cao X Y, Chan W J, Sun H X, Li A. Research progress on conjugated microporous polymer[J]. New Chemical Materials, 2024, 52(1): 243.

[15] Kang J Y, Shi Y P. Recent advances in research on sample pretreatment methods based on supramolecular

derived porous organic polymers[J]. Chinese Journal of Chromatography, 2024, 42(6): 496.
[16] Oleg T, Arthur J O. AutoDock Vina: Improving the speed and accuracy of docking with a new scoring function, efficient optimization, and multithreading[J]. Journal of Computational Chemistry, 2010, 31(2): 455.
[17] iang W, Cui W R, Liang R P, Qiu J D. Difunctional covalent organic framework hybrid material for synergistic adsorption and selective removal of fluoroquinolone antibiotics[J]. Journal of Hazardous Materials, 2021, 413: 125302.
[18] Oh H, Kim D, Kim D, Park I H, Jung O S. 2D porous organic templates via cocrystallization of melamine with disulfonic acids: adsorption of various alcohols in SCSC Mode[J]. Crystal Growth & Design, 2020, 20(10): 7027.
[19] Ahmed I, Tong M, Jun J W, Zhong C, Jhung S H. Adsorption of nitrogen-containing compounds from model fuel over sulfonated metal-organic framework: contribution of hydrogen-bonding and acid-base interactions in adsorption[J]. Journal of Physical Chemistry C, 2015, 120(1): 407.
[20] Lu T. A comprehensive electron wavefunction analysis toolbox for chemists, Multiwfn[J]. Journal of Chemical Physics, 2024, 161: 082503.
[21] Wu H, Liu Y L, Chang J Z, Zhao B X, Huo Y X, Wang Z L, Shi Y T. Extraction of five fluoroquinolones in eggs by magnetic solid-phase extraction with Fe_3O_4-MoS_2 and determination by HPLC-UV[J]. Food Analytical Methods, 2019, 12(3): 712.
[22] Li J, Zhou Y, Sun Z, Cai T, Wang X, Zhao S, Gong B. Restricted access media-imprinted nanomaterials based on a metal-organic framework for highly selective extraction of fluoroquinolones in milk and river water[J]. Journal of Chromatography A, 2020, 1626: 461364.
[23] Wei X, Chen Y Y, Zhong J Q, Zhu X P, Ren W, Zhao P. Determination of quinolone antibiotics in water by SiO_2/$MnFe_2O_4$ magnetic solid phase extraction-high performance liquid chromatography[J]. Chinese Journal of Analysis Laboratory, 2024, 43(5): 627.
[24] Wei Xiao, Chen Yuying, Zhong Jiaqi, Zhu Xiaping, Ren Wei, Zhao Ping. Determination of quinolone antibiotics in water by SiO_2/$MnFe_2O_4$ magnetic solid phase extraction-high performance liquid chromatography[J]. Chinese Journal of Analysis Laboratory, 2024, 43(5): 627.)
[25] Lu H Z, Chen Z R, Xu S F. Surface molecularly imprinted polymers on multi-function MnO_2-decorated magnetic carbon nanotubes for dispersive solid-phase extraction of three fluoroquinolones from milk samples[J]. ACS Food Science & Technology, 2022, 2(10): 1612.
[26] Bayatloo M R, Salehpour N, Alavi A, Nojavan S. Introduction of maltodextrin nanosponges as green extraction phases: Magnetic solid phase extraction of fluoroquinolones[J]. Carbohydrate Polymers, 2022, 297: 119992.
[27] Liu C, Liao Y M, Huang X J. Preparation of a boronic acid functionalized magnetic adsorbent for sensitive analysis of fluoroquinolones in environmental water samples[J]. Analytical Methods, 2016, 8(23): 4744.
[28] Fan Y M, Zeng G L, Ma X G. Multi-templates surface molecularly imprinted polymer for rapid separation and analysis of quinolones in water[J]. Environmental Science and Pollution Research, 2020, 27: 7177.
[29] Guan S P, Wu H, Yang L, Wang Z L, Wu J M. Use of a magnetic covalent organic framework material with a large specific surface area as an effective adsorbent for the extraction and determination of six fluoroquinolone antibiotics by HPLC in milk sample[J]. Journal of Separation Science, 2020, 43(19): 3775.
[30] Yuan G N, Ma J P, Li Y K, Li S. Determination of eight sulfonamide antibiotics in water by magnetic solid-phase extraction-ultra performance liquid chromatography-tandem mass spectrometry based on covalent organic framework materials[J]. Chinese Journal of Chromatography, 2025, 43(8): 894.